

EXPERIMENTAL AND NUMERICAL INVESTIGATION INTO TEMPERATURE HISTORIES AND RESIDUAL STRESS DISTRIBUTIONS OF HIGH STRENGTH STEEL S690 WELDED H-SECTIONS

Xiao Liu^{1,2} and Kwok-Fai Chung^{1,2*}

¹ Department of Civil and Environmental Engineering,

² Chinese National Engineering Research Centre for Steel Construction (Hong Kong Branch)
The Hong Kong Polytechnic University, Hong Kong SAR, China

ABSTRACT

In order to exploit full structural benefits offered by high strength steel materials in construction, it is important to examine and quantify effects of welding on these steel materials for development of effective structural design. A systematic experimental and numerical investigation into thermal and mechanical responses in four S690 welded steel H-sections with different cross-sectional dimensions during and after welding was conducted.

During welding, surface temperatures of the welded sections at specific locations in close vicinity of welding lines were measured continuously using thermocouples. After welding, surface residual stresses in these welded sections were measured using an established hole-drilling method. Based on codified data and measured temperatures, three-dimensional finite element models with thermomechanical coupled analyses were established to simulate heat transfer from a welding arc onto the welded sections. After a careful calibration of predicted surface temperature histories of these sections against measured data, both through-thickness temperature and residual stress distributions of these sections were obtained. Predicted and measured surface residual stresses at specific locations of these sections were found to be in a good agreement. Hence, accuracy of the proposed models in predicting temperature histories and residual stress distributions of these welded sections are established. Moreover, averaged through-thickness residual stresses are provided as representative residual stress patterns for these sections. It should be noted that the maximum residual stresses in these welded sections are proportionally smaller than those in S355 welded sections.

Consequently, the proposed finite element models are demonstrated to be able to predict accurate temperature histories and residual stress distributions of S690 welded H-sections through thermomechanical coupled analyses. The proposed models will be readily employed to investigate welding-induced residual stresses in welded H-sections and I-sections of various steel grades and plate thicknesses with different welding parameters. Predicted residual stress patterns will then be employed for numerical investigation into i) axial buckling behavior of slender columns made of S690 welded H-sections, and ii) lateral torsional buckling of unrestrained beams made of S690 welded I-sections. These numerical investigations will be reported separately.

Keywords: High strength steel, Welded H-sections, Temperature measurements, Residual stress distributions, Hole-drilling method, thermomechanical coupled analysis.

1. INTRODUCTION

For decades, common structural steel materials with yield strengths ranging from 235 to 355 N/mm², i.e. S235 to S355 steel materials, have been used widely in construction of buildings, bridges and heavily loaded structures owing to their excellent and consistent mechanical properties. In the past twenty years, high strength S690 to S960 steel materials become available in many parts of the world, and they offer attractive structural solutions in reducing self-weights of multi-storey buildings and long span bridges.

Welding is generally considered to be a highly effective means of connecting steel plates and sections together to form a structure. During fabrication of steel structures, welding-induced residual stresses are always present in welded sections due to highly non-uniform temperature distributions followed by different cooling rates in various parts of the steel sections (Withers & Bhadeshia, 2001a & 2001b; Masubuchi, 2013). Although section resistances of these welded sections are unlikely to be reduced, residual stresses have an adverse effect on stiffness, and hence, stability of these welded sections.

In the past decades, many researchers conducted experimental investigations into residual stress patterns of S235 to S355 welded sections. A simplified residual stress pattern for S235 to S355 welded sections was recommended by an ECCS document (ECCS, 1976), and it has been widely adopted in many structural steel design codes (CEN, 2005a & 2005b). For S460 steel materials, Wang et al. (2012) conducted a series of residual stress measurements on three welded H-sections of different cross-sectional dimensions using both 11.5 and 21.5 mm thick steel plates; all these plates were flame-cut (FC). Moreover, Ban et al (2014) fabricated a total of eight H-sections made of S460 flame-cut steel plates, and cross-sectional residual stress distributions were measured using a conventional sectioning method. The residual stress patterns of these sections were found to be similar in shape, but significantly smaller, when compared with those corresponding residual stresses in the ECCS pattern. Hence, the ECCS pattern is generally considered to be rather conservative for S460 welded H-sections.

A number of studies have been conducted to investigate the residual stress patterns for high strength steel welded sections. It should be noted that Rasmussen & Hancock (1992 & 1995) measured compressive residual stresses in six welded H-sections made of universal-mill (UM) and flame-cut (FC) thick steel plates using the sectioning method; yield strengths of these steel plates were found to range from 660 to 705 N/mm². It was found that for welded H-sections with UM steel plates, compressive residual stresses at both flanges and webs of these sections decreased as their cross-sectional dimensions increased. However, for welded H-sections with FC steel plates, tensile residual stresses were found at flange tips of those sections. It should be noted that accuracy of maximum residual stresses measured in a flange of these sections was somehow uncertain as out of only four to five measurements in a whole flange, only one to two measurements were made near the flange/web junction where maximum stresses were expected to take place.

Recently, Lee et al. (2012a) investigated residual stress distributions near weld toes of a number of S690 welded T- and Y-joints through the use of a hole-drilling method according to ASTM E837 (ASTM, 2013). Li et al. (2015) measured residual stress distributions of three S690 welded H-sections with 16 mm thick FC plates while their overall cross-sectional dimensions were found to range from 200 to 250 mm. When compared with the ECCS pattern for S235 to S355 welded steel sections, both tensile and compressive residual stress ratios at the flanges and the webs were found to be significantly smaller in magnitude. It should be noted that these sections were fabricated with gas metal arc welding (GMAW) with 2 number of passes per weld legs. It was concluded that the ECCS pattern was very conservative for S690 welded sections.

For numerical investigation, three dimensional finite element modelling according to computational welding mechanics (Goldak & Akhlaghi, 2006) was widely adopted to simulate welding of steel sections. Thermomechanical coupled analysis on finite element models were employed to simulate welding-induced thermal and mechanical responses of steel sections during welding as well as after welding. For computation of heat transfer during welding, a double ellipsoidal model proposed by Goldak et al. (1984) was widely adopted as an effective heat source model to simulate a welding arc. Through this heat source model, the heat energy was distributed into a double ellipsoid with two different semi-axis values in the front and the rear hemispheres. For computation of welding-induced residual stresses, various thermal properties such as thermal conductivity, specific heat capacity, and thermal expansion coefficient of steel materials at elevated temperatures were adopted. It should be noted that three dimensional finite element models were generally required to obtain both temperatures and residual stresses with a certain level of accuracy though they were very time-consuming (Duranton et al., 2004; Gery et al., 2005; Lee et al., 2012b).

In general, many researchers examined residual stresses and their effects on welded sections made of steel plates with yield strengths up to 460 N/mm² while only limited information on residual stresses in S690 welded sections is available so far. Hence, it is necessary to investigate thermal and mechanical responses of S690 welded sections during and after welding, and to quantify both magnitudes and distributions of residual stresses.

1.1 Objectives and scope of work

In order to exploit full structural benefits offered by high strength steel materials in construction, it is important to examine and quantify effects of welding on these steel materials for development of effective structural design. A systematic experimental and numerical investigation into thermal and mechanical responses in S690 welded steel H-sections was undertaken, and the investigation took the following forms of activities:

Task A Experimental investigation

- Task A1
High strength S690 steel plates of three different thicknesses were employed to fabricate four welded H-sections of different cross-sectional dimensions.

- Task A2
During welding, surface temperature histories of these four welded H-sections at specific locations in close vicinity of flange/web junctions were measured continuously using thermocouples.
- Task A3
After welding, surface residual stresses in these four welded H-sections were measured using the hole-drilling method according to ASTM E837 (ASTM, 2013).

Task B Numerical investigation

- Task B1
Based on codified data given in EN 1993-1-2, three-dimensional finite element models with thermomechanical coupled analyses for these four welded H-sections were established using ABAQUS (Version 6.12, 2009) to i) simulate heat transfer from a welding arc onto the flange/web junctions during welding, and ii) predict mechanical responses due to differential expansion and contraction within the welded sections after welding.
- Task B2
Comparison between measured and predicted surface residual stresses of these four welded H-sections was carried out, and averaged through-thickness residual stresses for these sections were provided.

The areas of interest of the present investigation are:

- through-thickness variations in temperatures as well as residual stresses in vicinity of flange/web junctions;
- equilibrium of forces based on welding-induced residual stresses developed over cross-sectional areas of the flange and the web in a flange/web junction; and
- representative residual stress patterns for welded H-sections.

2. EXPERIMENTAL INVESTIGATION

2.1. Test programme

A total of four S690 welded H-sections with different cross-sectional dimensions, namely, Sections C1 to C4 were tested. It should be noted that these sections were fabricated with S690 steel plates of three different thicknesses, i.e. 6, 10 and 16 mm using two different welding methods, namely i) Gas metal arc welding (GMAW), and ii) Submerged arc welding (SAW). Table 1 summarizes the test programme of the experimental investigation while cross-sectional dimensions of these sections are shown in Figure 1.

2.2. Material properties of S690 steel plates

In order to obtain material properties of S690 steel plates, a total of nine tensile tests were carried out in accordance with EN ISO 6892-1 (CEN, 2009). Measured stress-strain curves are plotted in Figure

2, and mechanical properties of the steel plates are summarized in Table 2. It should be noted that EN 1993-1-12 (CEN, 2007) specifies the following ductility criteria for steel materials with steel grades from S460 up to S700:

- i) tensile to yield strength ratio: $f_u / f_y \geq 1.05$;
- ii) elongation at fracture: $\epsilon_f \geq 10 \%$; and
- iii) elongation at f_u : $\epsilon_u \geq 15 f_y / E$.

It is shown that all the steel plates satisfy these ductility criteria, and they are readily qualified to be high strength steel materials to EN 1993-1-1 and 12. Moreover, matching welding materials with mechanical properties similar to those of the steel plates, as shown in Table 2, were selected accordingly for welding of these sections.

2.3. Welding procedures

Figure 3 illustrates the two different welding processes adopted in fabrication of welded H-sections. In each H-section, a total of four fillet weld runs were carried out, and a pre-heating temperature between 120 to 150 °C was adopted in order to prevent cold hydrogen cracking (AWS, 2011).

It should be noted that GMAW was conducted semi-automatically by qualified welders while SAW was conducted with an automatic machine by qualified welding operators. The welding wires CHW-80C1 (1.2 mm) and CHW-S80 (4.0 mm) were employed for GMAW and SAW respectively according to AWS A5.28 (AWS, 2005) and AWS A5.23M (AWS, 2011). Detailed welding parameters of the two processes are presented in Table 3. It should be noted that the line heat input energy of SAW is about twice of that of GMAW owing to increased plate thicknesses.

2.4 Temperature measurement

For each of the four welded H-sections, a total of nine thermocouples, namely, T1 to T9, were attached to specific locations at the top surface of the section flange, as shown in Figure 4. The thermocouples were provided to measure surface temperatures of these locations continuously during each weld run. It should be noted that the thermocouples were specified with an accuracy within $\pm 1.5^\circ\text{C}$, and a work range up to 1200°C.

Figure 5 plots typical temperature histories measured by these thermocouples during different weld runs. It should be noted that for weld run 2, the first group of thermocouples, namely, T1, T2 and T3, registered temperature change when the welding arc approached. After a certain time delay, the second group of thermocouples, T4, T5 and T6 registered approach of the welding arc, and this process repeated for the third group of thermocouples, T7, T8 and T9, after another time delay. Similar temperature measurements were also obtained from weld run 3. As the welding parameters of SAW were controlled to vary within small ranges in each weld run, the values of the maximum temperatures measured by these thermocouples in weld runs 2 and 3 are shown to be fairly close to each other.

It should be noted that during welding, the maximum temperature in the molten welding materials was about 1500 °C, and it was continuously deposited on the other side of the steel plate. Hence, a large transient temperature gradient existed through the thickness of the steel plate.

2.5 Residual stress measurement

The hole-drilling method recommended in ASTM E837 was adopted to measure residual strains of welded sections, and Figure 6 illustrates typical set-up of residual stress measurement. Small and shallow holes were drilled in specific locations of welded sections with a high speed hole drilling machine, as shown in Figure 7, to release any surface residual strain. To be specific, a 1.60 mm diameter tungsten carbide drill bit was used to drill a hole with a diameter of 2.00 mm over a depth of 2.00 mm in 8 equal increments in order to release all the surface residual strains of steel plates steadily. In general, these holes were considered to cause little adverse impact on integrity of structural members (Withers & Bhadeshia, 2001a), and these changes in surface residual strains were measured with circular rosettes. Comparing with the conventional sectioning method, this method was considered to be relatively simple, and yet sufficiently accurate in measuring residual strains in welded sections.

For each of the four welded H-section in the present investigation, a sufficiently large number of circular rosettes were installed at regular intervals on the outer surfaces of the flanges as well as on both sides of the web plate of the section, that is on ‘TF’, ‘BF’, ‘LW’ and ‘RW’ surfaces of the section as shown in Figure 8. Owing to different dimensions of the flange and the web plates, the total numbers of circular rosettes installed for Sections C1 to C4 were 32, 40, 48 and 64 respectively.

Hence, both released longitudinal strains, ε_x , and released transverse strains, ε_y , at specific locations of welded sections are measured after hole drilling, and the corresponding longitudinal and transverse residual stresses, f_{rx} and f_{ry} , at the location of the hole were readily calculated from the following:

$$\begin{cases} f_{rx} = E \cdot \frac{c_b(\varepsilon_x + \varepsilon_y) + c_a(\varepsilon_x - \varepsilon_y)}{4 c_a c_b} \\ f_{ry} = E \cdot \frac{c_b(\varepsilon_x + \varepsilon_y) - c_a(\varepsilon_x - \varepsilon_y)}{4 c_a c_b} \end{cases} \quad (1)$$

where E is the Young modulus of the steel material, and c_a and c_b are calibration coefficients measured experimentally based on ASTM E837 (Liu, 2017). Consequently, surface residual stresses at specific locations were calculated to provide comprehensive residual stress distributions in welded sections.

2.5.1 Residual stress distributions

After data analysis on released residual strains of all the four welded H-sections, Table 4 presents typical measured surface residual stresses for Section C3. It should be noted that large tensile surface residual stresses are found at the close vicinity of the centerlines of both the top and the bottom flanges

while relatively small compressive surface residual stresses are found elsewhere in the flanges. Owing to difficulty in measuring surface residual stresses in the webs near the top and the bottom flange/web junctions, measurements were only possible to be made in the central portions of the webs. In general, only relatively small compressive surface residual stresses are found. The measured surface residual stresses of Sections C1 to C4 are presented in Figure 9 for easy reference.

Key measured surface residual stresses of Sections C1 to C4 are summarized in Table 5, and it should be noted that:

- a) The maximum tensile stresses in the flanges are found to range from 354 to 452 N/mm², i.e. 0.44 to 0.60 of the measured yield strengths of the respective S690 steel plates.
- b) The maximum compressive stresses in the flanges are found to range from -146 to -267 N/mm², i.e. -0.18 to -0.35 of the measured yield strengths of the respective S690 steel plates.
- c) The maximum compressive stresses in the webs are found to range from -86 to -177 N/mm², i.e. -0.11 to -0.23 of the measured yield strengths of the respective S690 steel plates.

In order to compare with conventionally established values of residual stresses developed for S235 to S355 welded sections, residual stress ratios given in the ECCS pattern (ECCS, 1976) are also provided in Table 5 for direct comparison. It is shown that the measured surface residual stresses of these four S690 welded H-sections are significantly smaller than those of the established values. However, as there are large through-thickness temperature gradients in these welded sections, similar through-thickness variations in welding-induced residual stresses are expected. Hence, surface residual stresses should not be used as representative residual stresses for S690 welded sections as large variations within plate thicknesses are expected.

3. NUMERICAL INVESTIGATION

In order to obtain representative residual stresses of S690 welded sections, a systematic numerical investigation was carried out to establish welding induced thermal and mechanical responses of these sections. Thermomechanical coupled analyses were adopted to simulate effects of welding to the four welded H-sections as shown in Figure 1 to predict their temperature histories and residual stress distributions. A “Birth and Death” technique was employed to simulate deposition of molten welding materials in each welding run.

It should be noted that a three-dimensional eight-noded linear solid element, Element C3D8RT, was used for thermomechanical coupled analyses. With a formulation of reduced integration, there was only one integration point at the centre of the solid element, and hence, this element required minimal computational time. Moreover, four layers of elements were adopted within the thickness of the steel plates, and this was considered to be effective to avoid potential hour-glass problems.

3.1. Material and mechanical properties at elevated temperatures

According to ASM Material Handbook (Davis, 1990) and EN 1993-1-2 (CEN, 2005b), temperature-dependent thermal properties such as thermal conductivity, specific heat capacity, and coefficient of thermal expansion were incorporated into the finite element models. These thermal properties are illustrated in Figure 10. For simplicity, the radiation emissivity ξ_{res} and the film coefficient α for radiation are taken to be 0.5 and 15 W/m²/K respectively.

In order to predict mechanical responses of these welded H-sections accurately during thermomechanical coupled analyses, true stress-strain relationships for S690 steel plates derived from tensile tests were adopted. These relationships for steel plates of different thicknesses are plotted in Figure 11. However, there is a lack of mechanical properties of S690 steel plates at elevated temperatures. For simplicity, reduction factors to both yield strength and Young's modulus of S235 to S460 steel plates at elevated temperatures given in EN 1993-1-2 (CEN, 2005b) and ASM Material Handbook (Davis, 1990), as shown in Figure 12, are adopted in the proposed finite element model.

3.2. Heat source model

It is very important to model heat transfer of a welding arc accurately during welding, the double ellipsoidal suggested by Goldak et al (1984) was employed to simulate the moving welding arc, as shown in Figure 13. It should be noted that all the parameters of the proposed double ellipsoidal for these four welded H-sections are summarized in Table 6. Hence, the volumetric heat flux in respective of the front and the rear hemispheres of the double ellipsoid, q_1 and q_2 [W/m³] are given by:

$$\begin{cases} q_1(x, y, z) = \frac{6\sqrt{3}f_f Q}{a_1 b c \sqrt{\pi}} \exp\left(-\frac{3x^2}{a_1^2}\right) \exp\left(-\frac{3y^2}{b^2}\right) \exp\left(-\frac{3z^2}{c^2}\right) \\ q_2(x, y, z) = \frac{6\sqrt{3}f_r Q}{a_2 b c \sqrt{\pi}} \exp\left(-\frac{3x^2}{a_2^2}\right) \exp\left(-\frac{3y^2}{b^2}\right) \exp\left(-\frac{3z^2}{c^2}\right) \end{cases} \quad (2)$$

where

$a_1, a_2, b,$ and c are semi-axes of the double ellipsoid [m];

Q is the total heat input energy of the welding arc, where $Q = \eta \cdot U \cdot I$ [J];

$x, y,$ and z are the local coordinates as shown in Figure 13; and

f_f and f_r are fractions illustrating energy distribution, hence, $f_f + f_r = 2$.

In general, dimensions $a_1, a_2, b,$ and c of the proposed double ellipsoidal are specified after a careful consideration on

- i) line heat input energy for each weld run according to the welding procedures given in Table 3,
- ii) predicted temperatures at specific measuring points of the flanges, and
- iii) sizes and shapes of the molten welding materials through trials and errors.

As Sections C1 and C2 were fabricated with GMAW while Sections C3 and C4 were fabricated with SAW, two different sets of parameters were proposed. In general, dimensions a_1 , a_2 , b , and c of the double ellipsoidal for SAW are larger than those for GMAW, due to the use of a large electric current.

3.3. Convergence study

In order to establish numerical convergence of the proposed finite element models in performing thermomechanical coupled analyses, a total of six models with different mesh configurations of Section C1, namely Models C1-a to C1-f, have been analyzed. The convergence study is summarized in Table 7 while the finite element models with different mesh configurations are illustrated in Figure 14 for easy comparison. In general, the mesh sizes in the flange/web junctions are steadily decreased from Models C1-a to C1-f. As a result, the total numbers of elements are increased correspondingly from 1,218 in Model C1-a to 92,700 in Model C1-f.

Table 8 summarizes surface temperatures and surface residual stresses at the centre-line of the flange/web junction of these six models. It is found that Model C1-a cannot predict residual stresses rationally as there is only one layer of elements across the plate thickness. From Models C1-b to C1-f, the surface temperatures are found to increase from 505 °C to 511 °C from Model C1-b to C1-f while the corresponding surface residual stresses are found to increase from +392 to +434 N/mm². Moreover, the corresponding total tensile forces of the flange/web junction are found to increase from 151 to 167 kN. In order to achieve a high numerical accuracy with a reasonable computational time, the mesh configuration of Model C1-d is adopted for subsequent analyses. It should be noted that convergence in residual stresses is more critical than that in temperatures.

3.4. Calibration of finite element models

After establishing convergence of the models, systematic thermomechanical coupled analyses of the models for Sections C1 to C4 were carried out. Measured temperature histories and residual stress distributions obtained in the experimental investigation were employed to calibrate the proposed finite element models.

3.4.1. Temperature distributions and histories

Figure 15 illustrates typical transient temperature distributions of the proposed model during welding. Two sectional views of the bottom flange/web junction are provided to illustrate maximum temperature distributions for different weld runs. It should be noted that the grey regions shown in the vicinity of the flange/web junction represent molten welding material being deposited during welding, and their temperatures exceed 1,500 °C. More importantly, it is shown that large temperature gradients exist within the flange/web junction, and the temperatures at the out surface of the flange range typically from 450 to 550 °C. Figure 16 plots both measured and predicted surface temperature histories at specific locations, i.e. at various measuring points of thermocouples T1, T2 and T3 of the flange/web junction induced by two different weld runs. It is evident that the predicted surface temperatures compare very well to those corresponding measured data.

3.4.2. Residual stress distributions

Figure 17 illustrates typical residual stress distributions of the proposed finite element models of these welded H-sections after welding. It is shown that owing to the presence of large through-thickness temperature gradients in the flange/web junctions, through-thickness variations in their residual stresses are large. Moreover, the maximum residual stresses within the top and the bottom flange/web junctions associated with weld runs 3 and 4 are larger than those associated to weld runs 1 and 2. This is most likely caused by tempering effects provided by weld runs 3 and 4 onto those residual stresses associated with weld runs 1 and 2. Figure 18 illustrates three-dimensional plots of the predicted residual stresses for all the four welded H-sections, showing highly non-linear distributions of residual stresses within their flange/web junctions.

3.4.2.1 Numerical accuracy

In order to assess numerical accuracy of the proposed finite element models, Table 9 summarizes a comparison between measured and predicted surface residual stresses of one of the welded H-sections. It is shown that for Section C3, the predicted surface residual stresses in the outer surfaces of both the top and the bottom flanges compare very well with those measured values as the corresponding average errors are found to be merely 36 and 23 N/mm² respectively. Similarly, the predicted surface residual stresses in the left and the right surfaces of the web also compare very well with those measured values as the corresponding average errors are found to be merely 19 and 40 N/mm² respectively. Moreover, the average relative errors of various parts of the section were found to range from 2.5 to 5.3 % out of a total of 48 data. All of these average relative errors for various parts as well as the overall average values of these four welded H-sections are summarized in Table 10. As the overall average relative errors in predicted surface residual stresses are shown to range from 3.8 to 8.1 %, the proposed finite element models are thus considered to be highly acceptable.

Figure 19 plots the measured and the predicted surface residual stresses of Sections C1 to C4 onto the same graphs for direct comparison. It is shown that comparison between the measured and the predicted outer surface residual stresses in the flanges as well as the webs for each of the four sections are highly satisfactorily. It should be noted that the predicted inner surface residual stresses of the flanges and the webs of the sections are provided in these plots for direct comparison. Moreover, averaged through-thickness residual stresses are evaluated and presented as representative residual stress patterns for these sections.

3.4.2.2 Self-equilibrium of residual stresses

As residual stresses within a cross section should be self-equilibrated, it is essential to check force equilibrium over the cross section of each of these four welded sections to ensure that there is no out-of-balance force. Such a check is illustrated in Figure 20 for these sections in which compressive and tensile residual stresses over various parts of half of a cross-section (due to symmetry) are summed up and grouped together appropriately to demonstrate equilibrium. Among all cases, the out-of-balance forces are found to range merely from -0.4 to 6.7 kN while the total forces due to compressive

(or tensile) residual stresses are found to range from +222 to +454 kN. Hence, the predicted residual stress distributions in these sections are confirmed to be in self-equilibrium.

Consequently, the proposed finite element models are demonstrated to be able to predict accurate temperature histories and residual stress distributions of S690 welded H-sections through thermomechanical coupled analyses. The models have been calibrated successfully against measured data.

3.4.2.3 Comparison with design values

For direct comparison, the ECCS pattern for S235 to S355 welded sections, and the residual stress pattern of the proposed finite element models for S690 welded sections are illustrated in Figure 21. It is evident that these two patterns are similar in shape. More specifically, in both patterns, high tensile residual stresses exist at the flange/web junctions, and they are readily balanced by relatively small compressive residual stresses over the rest of the flanges and the central portion of the web.

In order to assess their relative residual stress levels, Table 11 summarizes these residual stress ratios for direct comparison according to different welding methods. It is shown that:

- For Sections C1 and C2, the maximum ratios given by the proposed models for tensile and compressive residual stresses in the flanges α^+ and α^- are +0.82 and -0.27 when compared with +1.0 and -0.5 given by the ECCS pattern correspondingly.
- For Sections C3 and C4, the maximum ratios given by the proposed models for tensile and compressive residual stresses in the flanges α^+ and α^- are +0.58 and -0.15, when compared with +1.0 and -0.5 given by the ECCS pattern correspondingly.
- Such large differences in these residual stress ratios among the four welded sections are mainly due to use of different welding methods, and different line heat input energies are provided to the flange/web junctions during welding.

Consequently, it is established that the residual stresses in S690 welded H-sections are proportionally less pronounced when compared with those recommended by the ECCS pattern. Hence, it is confirmed that the ECCS residual stress pattern for S235 to S355 welded sections are not applicable to S690 welded sections as the residual stresses will then be significantly over-estimated.

4. CONCLUSIONS

In order to exploit full structural benefits offered by high strength steel materials in construction, it is important to examine and quantify effects of welding on these steel materials for development of effective structural design. A systematic experimental and numerical investigation into thermal and mechanical responses in four S690 welded H-sections with different cross-sectional dimensions during and after welding was conducted. It is shown that:

- a) Surface temperature histories in welded H-sections were directly measured with well positioned thermocouples during welding, and they were successfully employed to calibrate the proposed finite element models with thermomechanical coupled analyses through comparison between measured and predicted temperatures.
- b) Surface residual strains in welded H-sections were systematically measured using the hole drilling method, and corresponding residual stresses were evaluated through the use of codified formulae. These surface residual stresses were successfully employed to calibrate the proposed finite element models through comparison between measured and predicted surface residual stresses.
- c) Averaged through-thickness residual stresses were provided as representative residual stress patterns for these S690 welded H-sections. It should be noted that the maximum residual stresses in these sections are proportionally smaller than those values given in the ECCS document for S235 to S355 welded sections.

Consequently, the proposed finite element models are demonstrated to be able to predict accurate temperature histories and residual stress distributions of S690 welded H-sections through thermomechanical coupled analyses. The proposed models will be readily employed to investigate welding-induced residual stresses in welded H-sections and I-sections of various steel grades and plate thicknesses with different welding parameters. The predicted residual stress patterns will then be employed for numerical investigation into i) axial buckling behavior of slender columns made of S690 welded H-sections, and ii) lateral torsional buckling of unrestrained beams made of S690 welded I-sections. These numerical investigations will be reported separately.

Acknowledgement

The authors are grateful to the financial support provided by the Research Grant Council of the Government of Hong Kong SAR (Project Nos. PolyU 5143/13E, and PolyU 152194/15E). The project leading to the publication of this paper is also partially funded by the Research Committee (Project No. RTK3) and the Chinese National Engineering Research Centre for Steel Construction (Hong Kong Branch) (Project No. 1-BBY3 & 6) of the Hong Kong Polytechnic University. The research studentship of the first author provided by the Hong Kong Polytechnic University are acknowledged.

Special thanks go to the Nanjing Iron and Steel Company Ltd. in Nanjing for supply of high strength steel materials, and the Pristine Steel Fabrication Company Ltd. in Dongguan for welding of steel sections. All residual stress measurements on welded H-sections were carried out at the Structural Engineering Research Laboratory of the Department of Civil and Environmental Engineering at the Hong Kong Polytechnic University, and supports from the technicians are gratefully acknowledged.

REFERENCES

- 1) AWS (2005). Specification for Low-Alloy Steel Electrodes and Rods for Gas Shielded Arc Welding. *Structural Welding Code – Steel*, American Welding Society, Miami, United States.
- 2) ABAQUS 6.12 (2009). Theory manual. Providence, US: Dassault Systemes Simulia Corp.
- 3) AWS (2011). Specification for Low-Alloy Steel Electrodes and Fluxes for Submerged Arc Welding. *Structural Welding Code – Steel*, American Welding Society, Miami, United States.
- 4) ASTM International (2013). Standard Test Method for Determining Residual Stresses by Hole-Drilling Strain-Gauge Method ASTM E837. *ASTM International*, West Conshohocken, United States.
- 5) Brown S & Song H (1992). Finite element simulation of welding of large structures. *Journal of Engineering for Industry*, 114(4), 441-451.
- 6) BJORHOLDE R (2004). Development and use of high performance steel. *Journal of Constructional Steel Research*, 60(3), 393-400.
- 7) BAN HY, SHI G, & SHI YJ (2014). Experimental and unified model investigations on residual stress within high strength steel welded I-sections. *Engineering Mechanics*, 31(8), 83-91.
- 8) CEN (2005a). EN-1993-1-1:2005, Eurocode 3: Design of steel structures – Part 1–1: General rules and rules for buildings. *European Committee for Standardization*, Brussels, Belgium.
- 9) CEN (2005b). EN-1993-1-2:2005, Eurocode 3: Design of steel structures – Part 1–2: General rules – Structural fire design. *European Committee for Standardization*, Brussels, Belgium.
- 10) CEN (2007). EN-1993-1-12:2007, Eurocode 3: Design of steel structures – Part 1–12: Additional rules for the extension of EN 1993 up to steel grades S700. *European Committee for Standardization*, Brussels, Belgium.
- 11) CEN (2009). BS EN ISO 6892-1, Metallic materials – Tensile testings, Part 1: Method of test at ambient temperature. *European Committee for Standardization*.
- 12) DAVIS JR (1990). Materials handbook. *American Society for Metals*, USA, 10th Edition., Vol. 1.
- 13) DURANTON P, DEVAUX J, ROBIN V, GILLES P & BERGHEAU JM (2004). 3D modelling of multi-pass welding of a 316L stainless steel pipe. *Journal of Materials Processing Technology*, 153, 457-463.
- 14) ECCS (1976). Manual on Stability of Steel Structures. *European Convention for Constructional Steelwork Publication*, 2nd Edition.
- 15) GOLDAK J, CHAKRAVARTI A & BIBBY M (1984). A new finite element model for welding heat sources. *Metallurgical Transactions B*, 15(2), 299-305.
- 16) GERY D, LONG H & MAROPOULOS P (2005). Effects of welding speed, energy input and heat source distribution on temperature variations in butt joint welding. *Journal of Materials Processing Technology*, 167(2), 393-401.
- 17) GOLDAK JA, AKHLAGHI M (2006). Computational Welding Mechanics. *Springer Science & Business Media*.
- 18) LEE CK, CHIEW SP & JIANG J (2012a). Residual stress study of welded high strength steel thin-walled plate-to-plate joints. Part 1: Experimental study. *Thin-Walled Structures*, 56, 103-112.

- 19) Lee CK, Chiew SP & Jiang J (2012b). Residual stress study of welded high strength steel thin-walled plate-to-plate joints. Part 2: Numerical modeling. *Thin-Walled Structures*, 59, 120-131.
- 20) Li TJ, Li GQ & Wang YB (2015). Residual stress tests of welded Q690 high-strength steel box- and H-sections. *Journal of Constructional Steel Research*, 115, 283-289.
- 21) Liu X & Chung KF (2016). Experimental Investigation into Residual Stresses of Welded H-sections Made of Q690 Steel Materials, *Proceeding of the Fourteenth East Asia-Pacific Conference*, Ho Chi Minh City, January 2016, p559-566.
- 22) Liu X (2017). Structural effects of welding onto high strength S690 steel plates and welded sections. *PhD Thesis*, Hong Kong.
- 23) Masubuchi K (2013) Analysis of welded structures: Residual stresses, distortion, and their consequences. *Elsevier*. Vol. 33.
- 24) Rasmussen K & Hancock G (1992). Plate slenderness limits for high strength steel sections. *Journal of Constructional Steel Research*, 23(1), 73-96.
- 25) Rasmussen K & Hancock G (1995). Tests of high strength steel columns. *Journal of Constructional Steel Research*, 34(1), 27-52.
- 26) Schmidt H & Hattel J (2004). A local model for the thermomechanical conditions in friction stir welding. *Modelling and Simulation in Materials Science and Engineering*, 13(1), 77.
- 27) Withers PJ & Bhadeshia HKDH (2001a). Residual stress. Part 1 – Measurement techniques. *Materials Science and Technology*, 17(4), 355-365.
- 28) Withers PJ & Bhadeshia HKDH (2001b). Residual stress. Part 2 – Nature and origins. *Materials Science and Technology*, 17(4), 366-375.
- 29) Willms R (2009). High strength steel for steel construction. *Proceedings of Nordic Steel Construction Conference*, pp. 597-604.
- 30) Wang YB, Li GQ & Chen SW (2012). Residual stresses in welded flame-cut high strength steel H-sections. *Journal of Constructional Steel Research*, 79, 159-165.

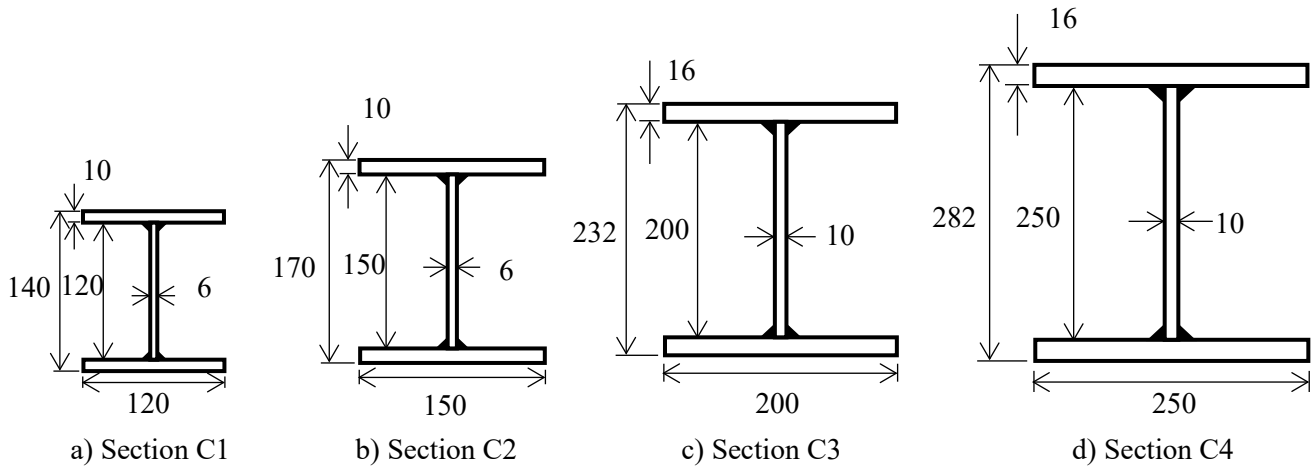


Figure 1. Cross-sectional dimensions of S690 welded H-sections

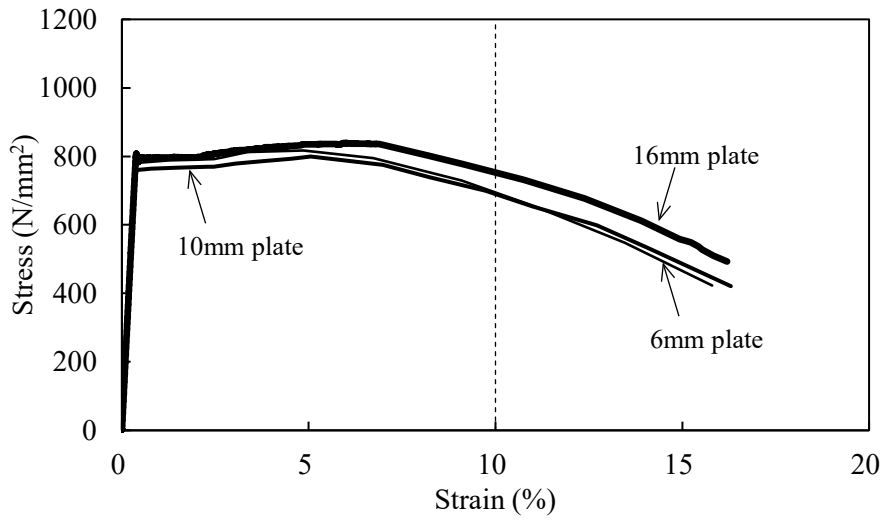
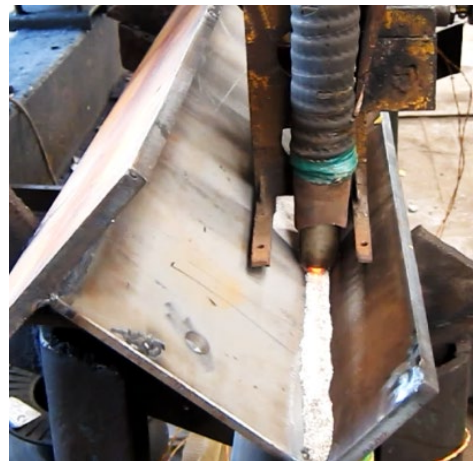


Figure 2. Measured stress-strain curves of S690 steel plates of different thicknesses



a) Gas metal arc welding (GMAW)



b) Submerged arc welding (SAW)

Figure 3. Welding processes

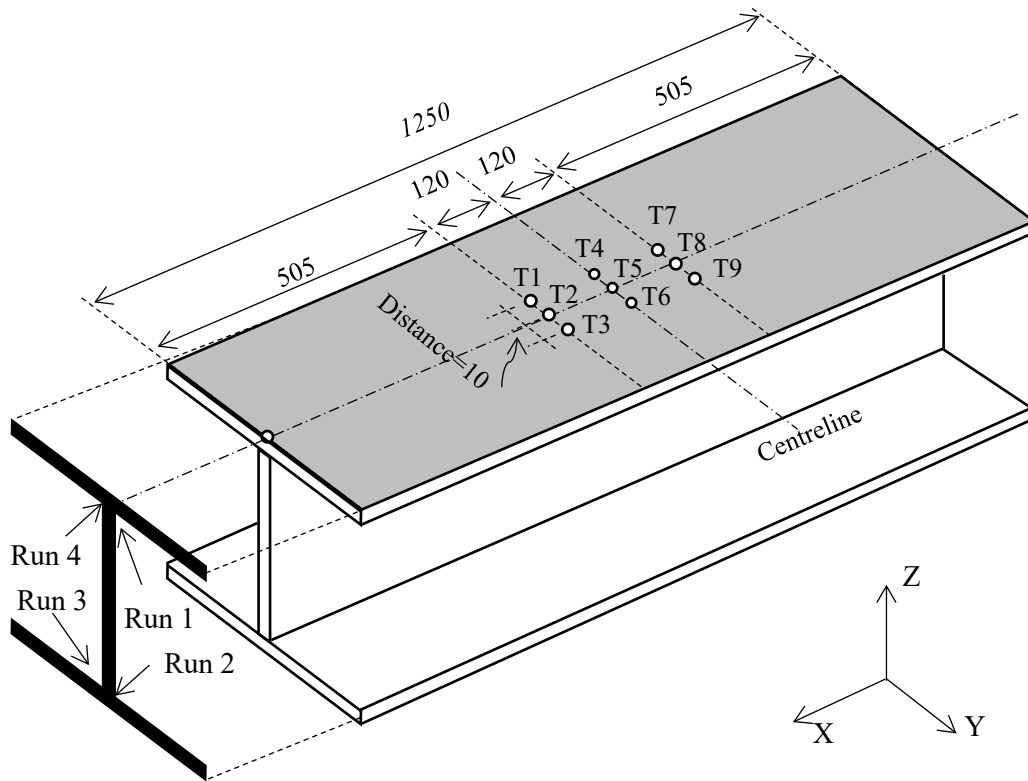
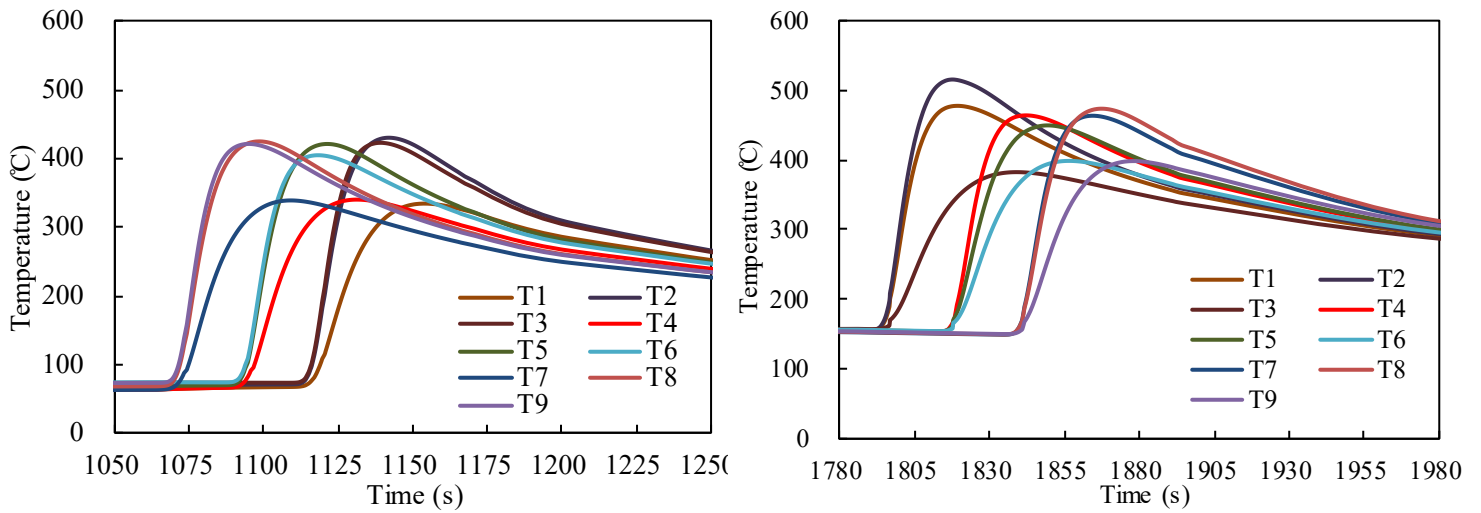


Figure 4. Schematic diagram of welding – Section C3



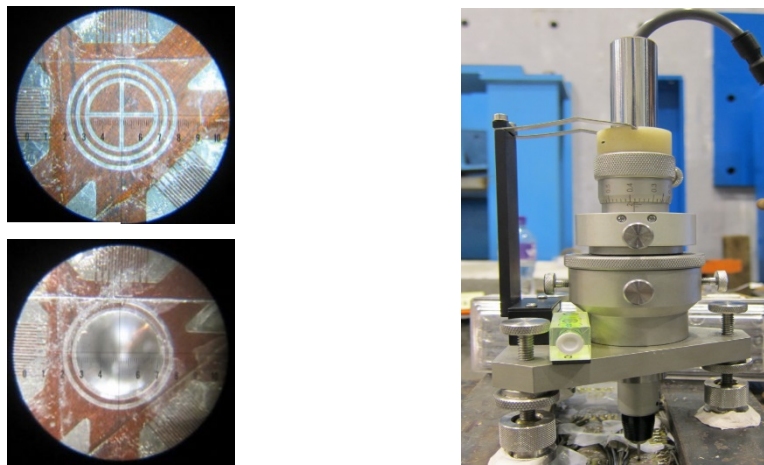
a) Weld run 2

b) Weld run 3

Figure 5. Temperature histories during welding run 2 and run 3 – Section C3



Figure 6. Test set-up for residual stress measurement – Section C3



a) Rosette before and after drilling b) High speed hole-drilling machine

Figure 7. Measuring residual stresses using the hole drilling method

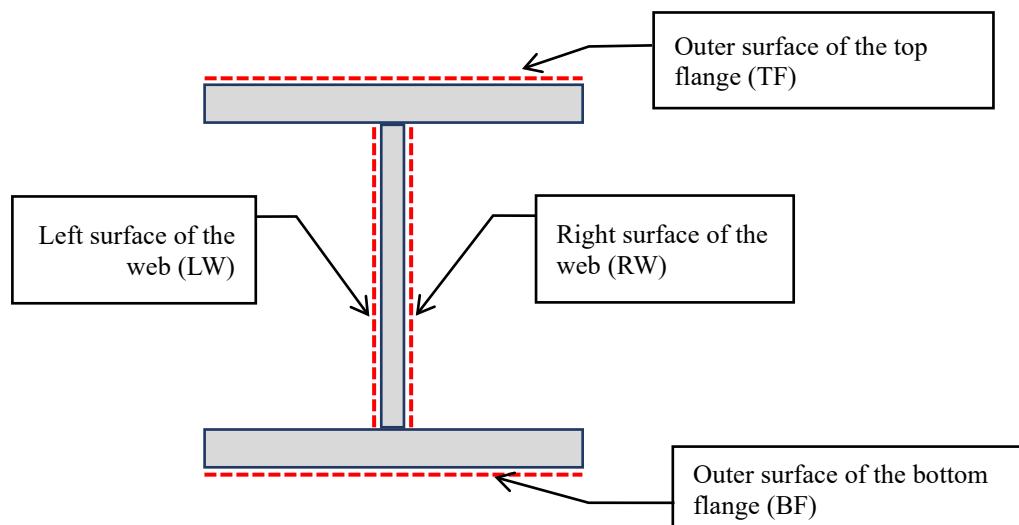


Figure 8. Arrangement of circular rosettes

Unit: N/mm^2

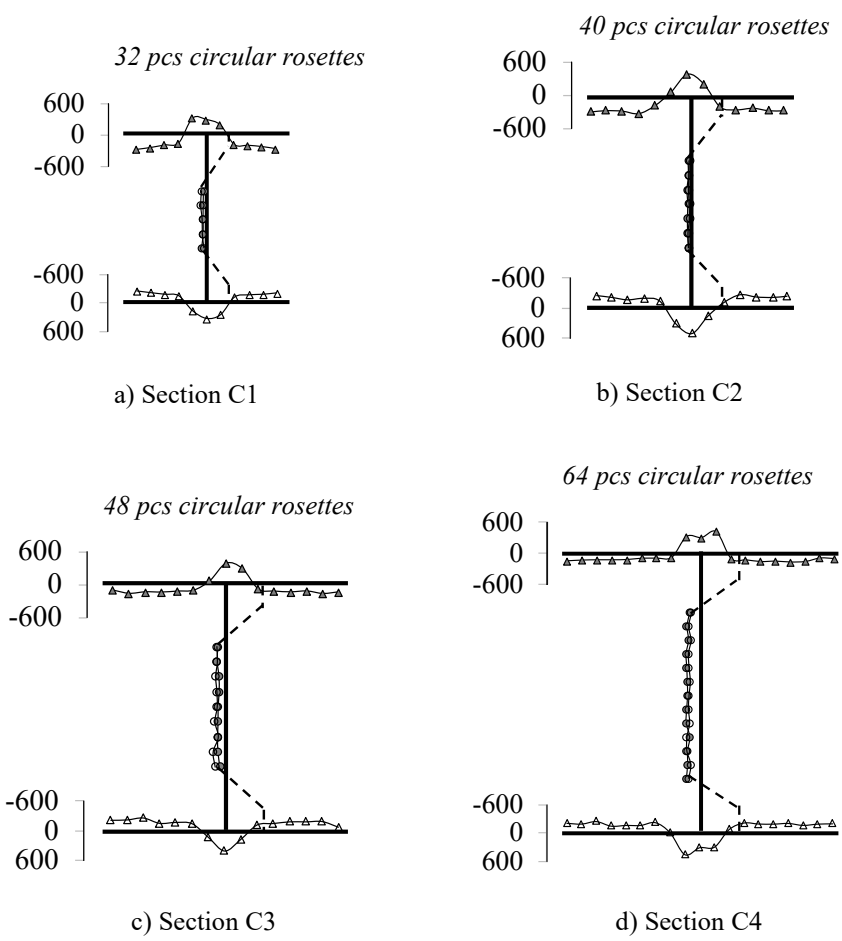


Figure 9. Cross-sectional distributions of measured residual stresses

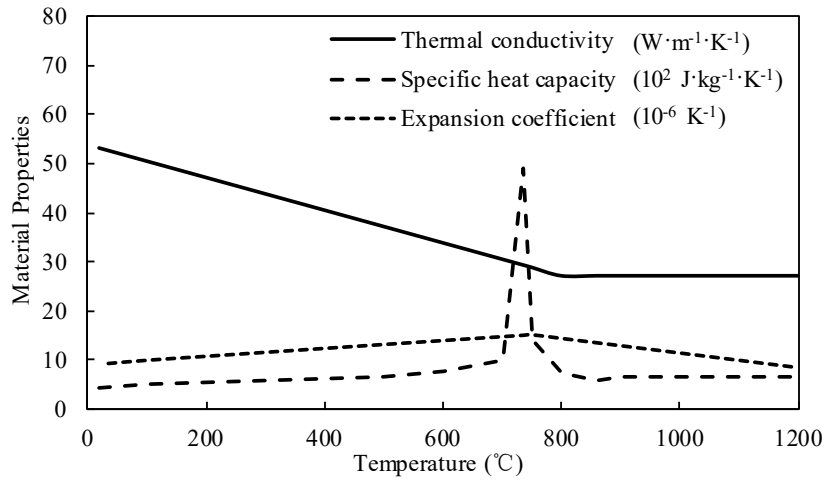


Figure 10. Non-linear thermal properties for S690 steel plates at elevated temperatures

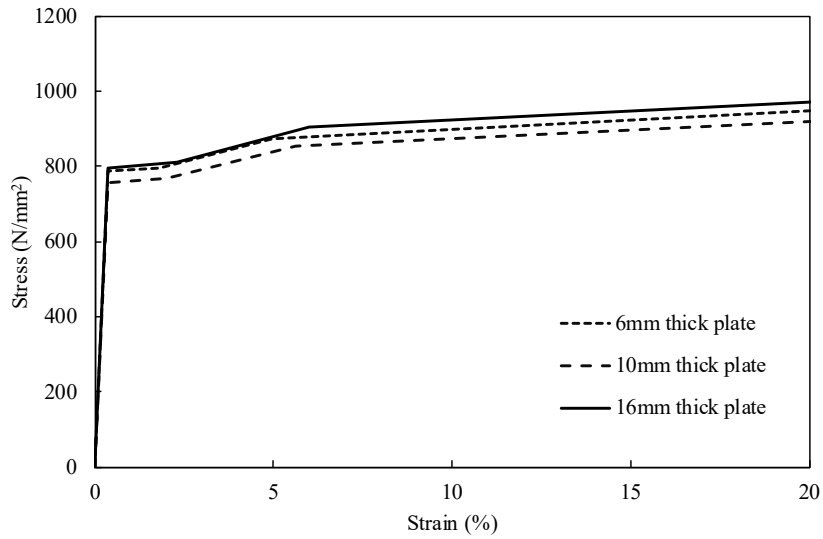


Figure 11. True stress-strain relationships for S690 steel plates at ambient temperature

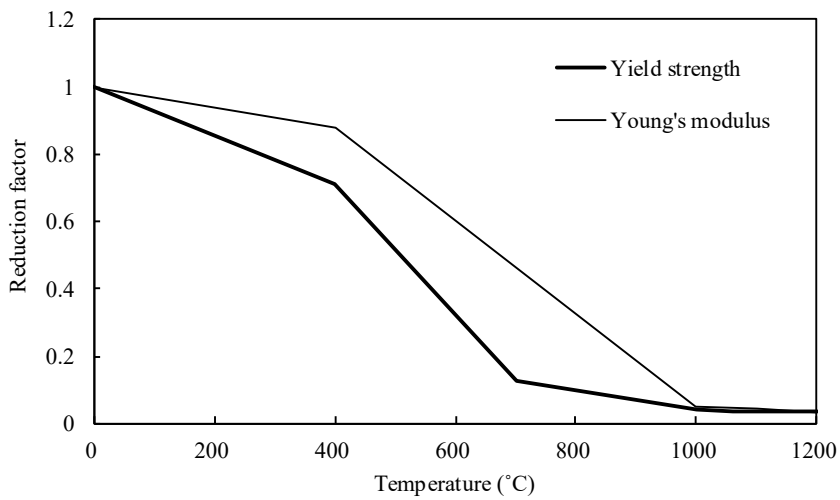


Figure 12. Reduction factors for S690 steel plates at elevated temperatures

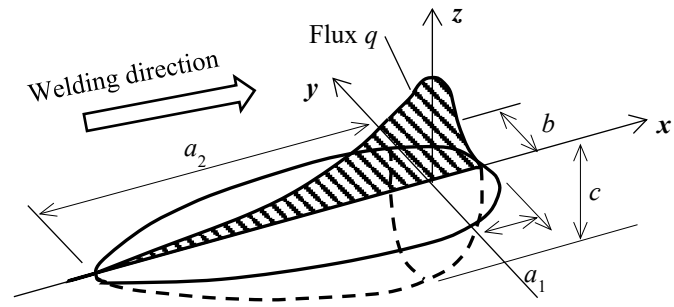


Figure 13. A double ellipsoidal as a heat source model

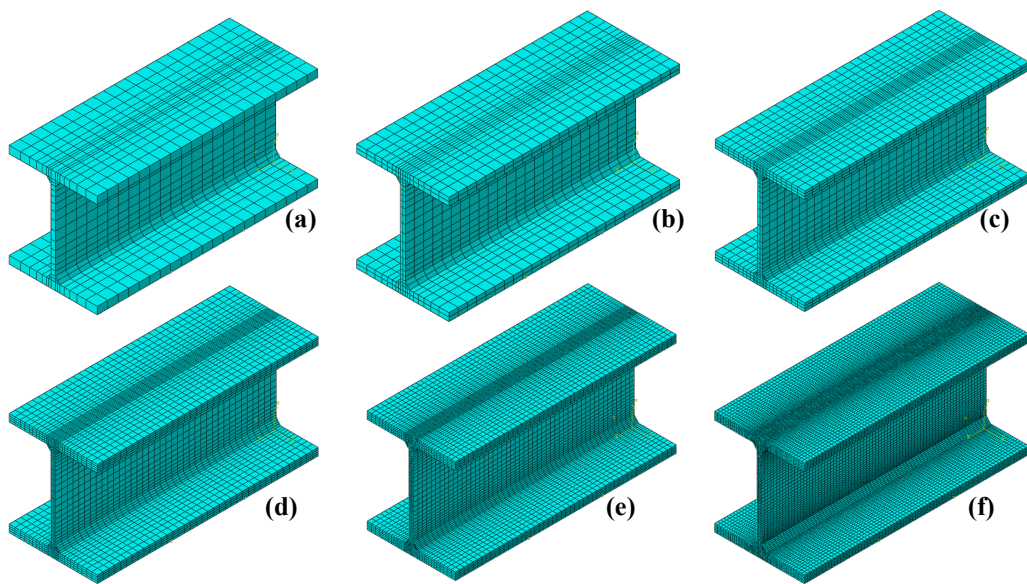


Figure 14. Three dimensional finite element models with different mesh configurations – Section C1

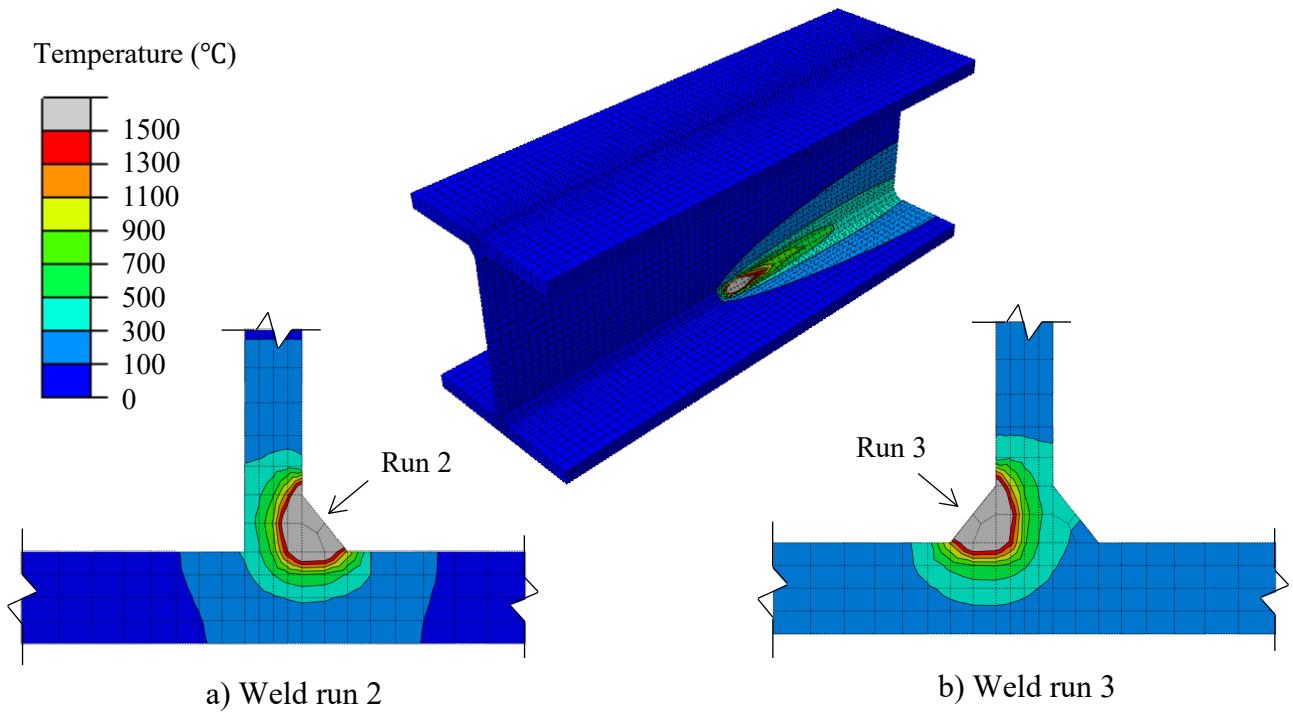


Figure 15. Transient temperature distributions in flange/web junction – Section C3

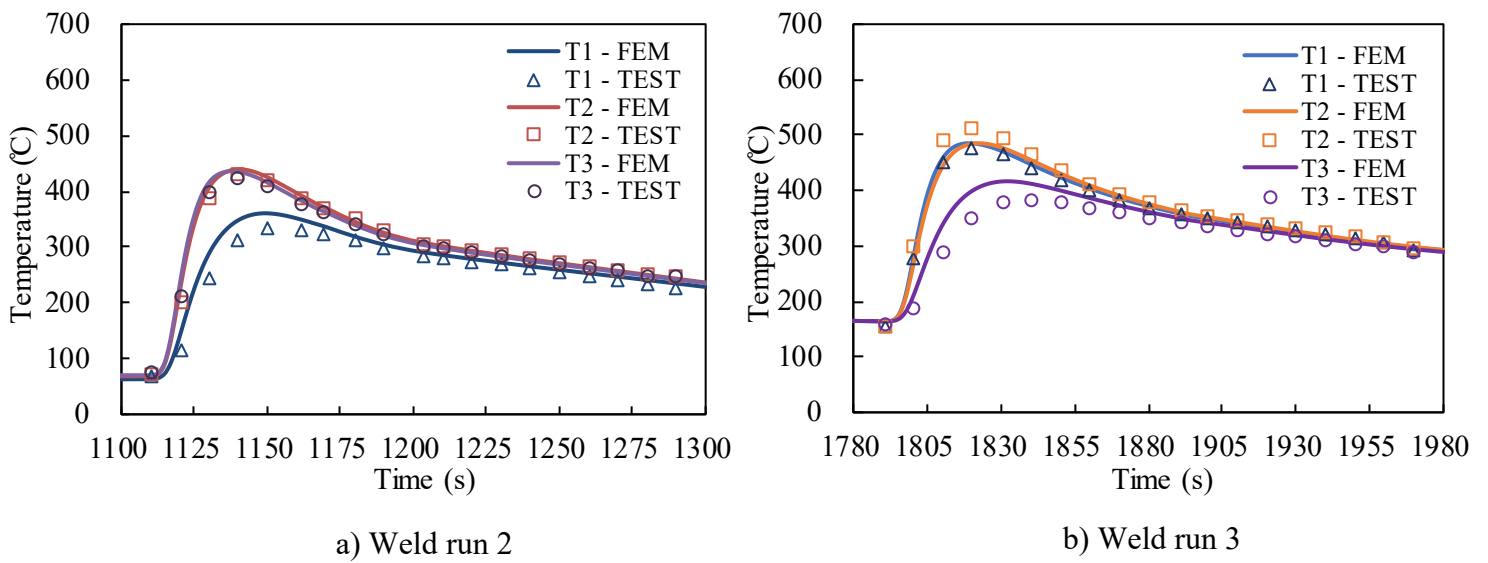


Figure 16. Comparison of measured and predicted temperature histories – Section C3

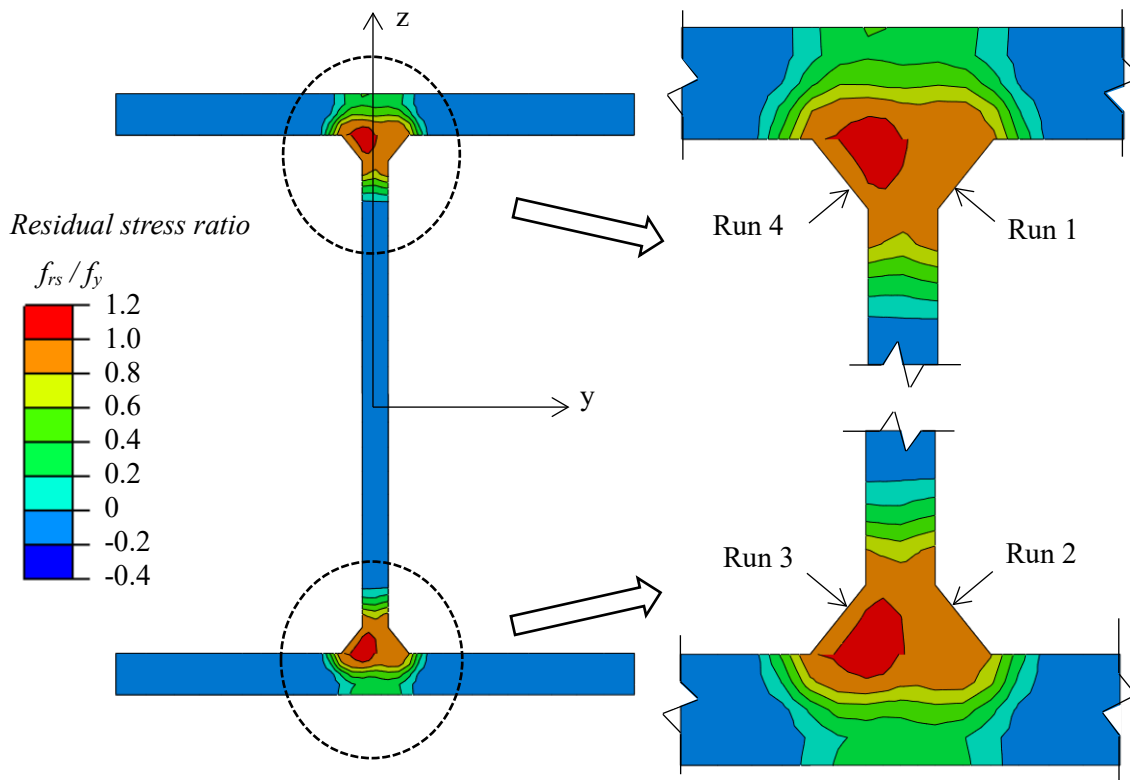


Figure 17. Cross-sectional distribution of residual stresses – Section C3

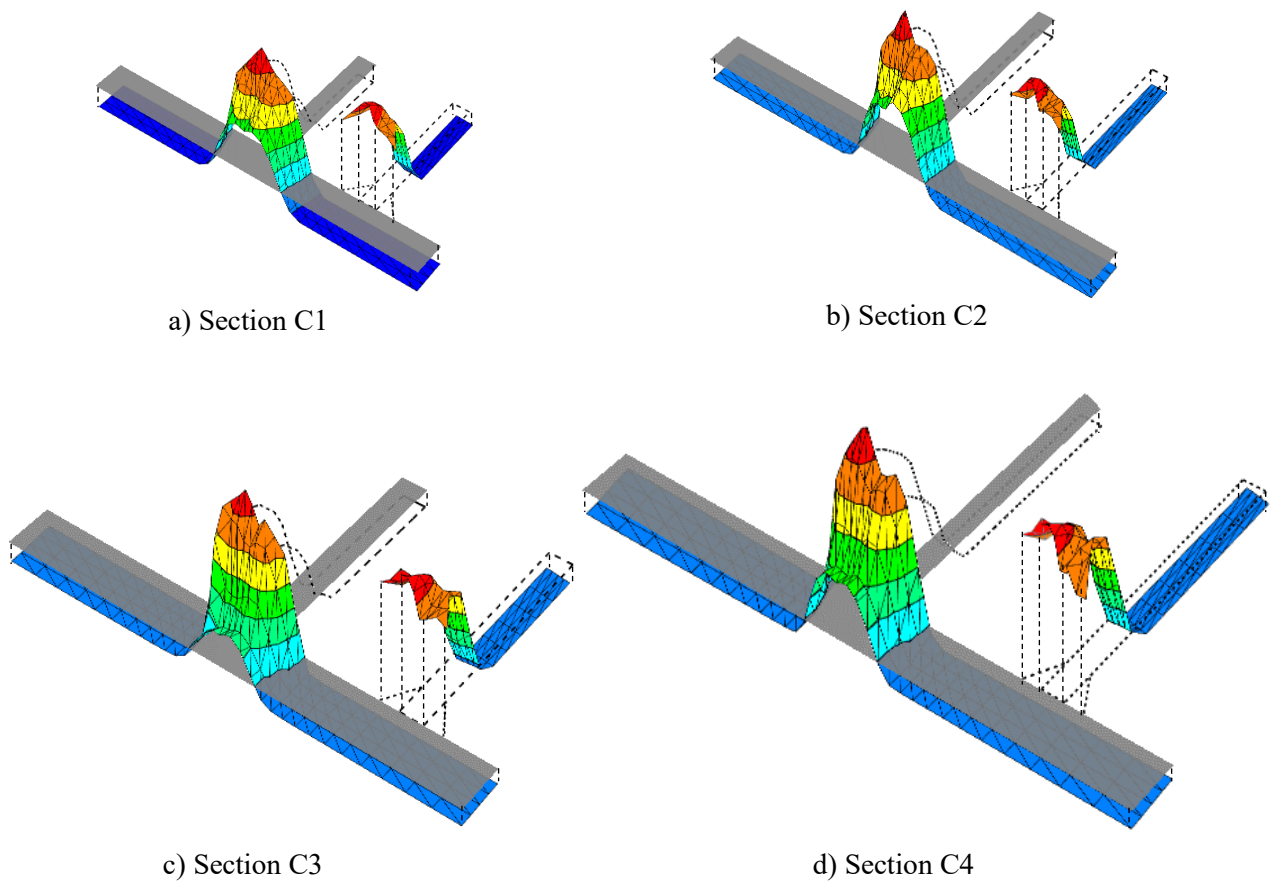


Figure 18. Three dimensional plots of predicted residual stresses in welded H-sections

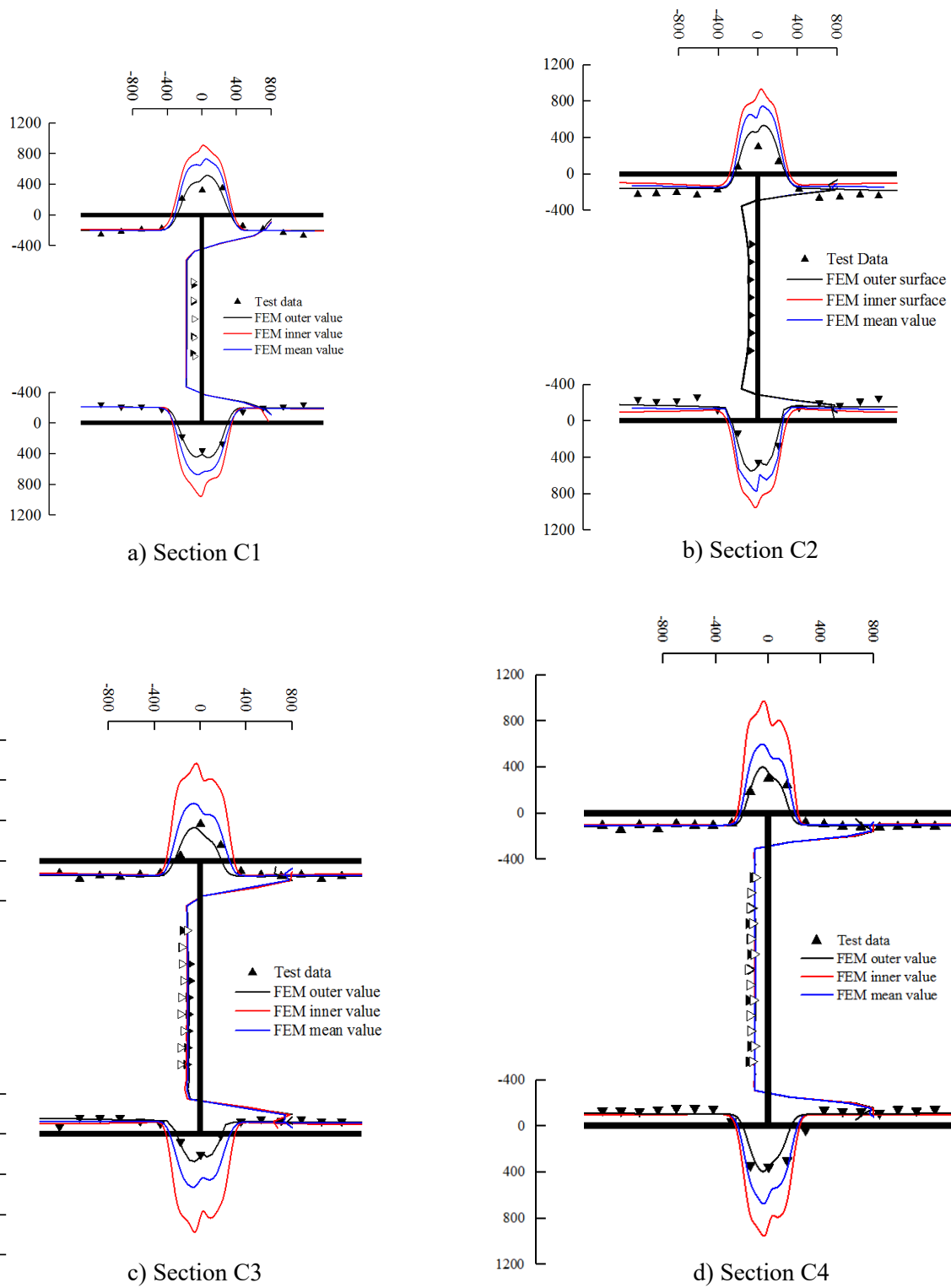


Figure 19. Comparison of measured and predicted residual stress distributions

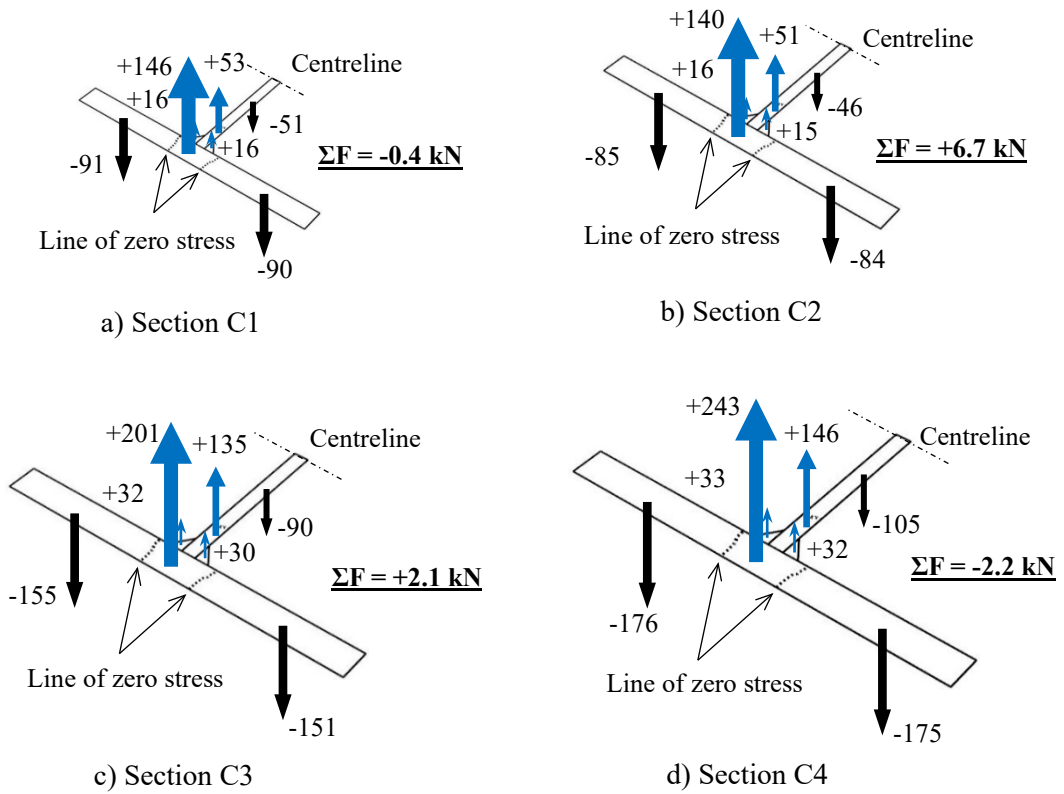


Figure 20. Force equilibrium in welded H-sections

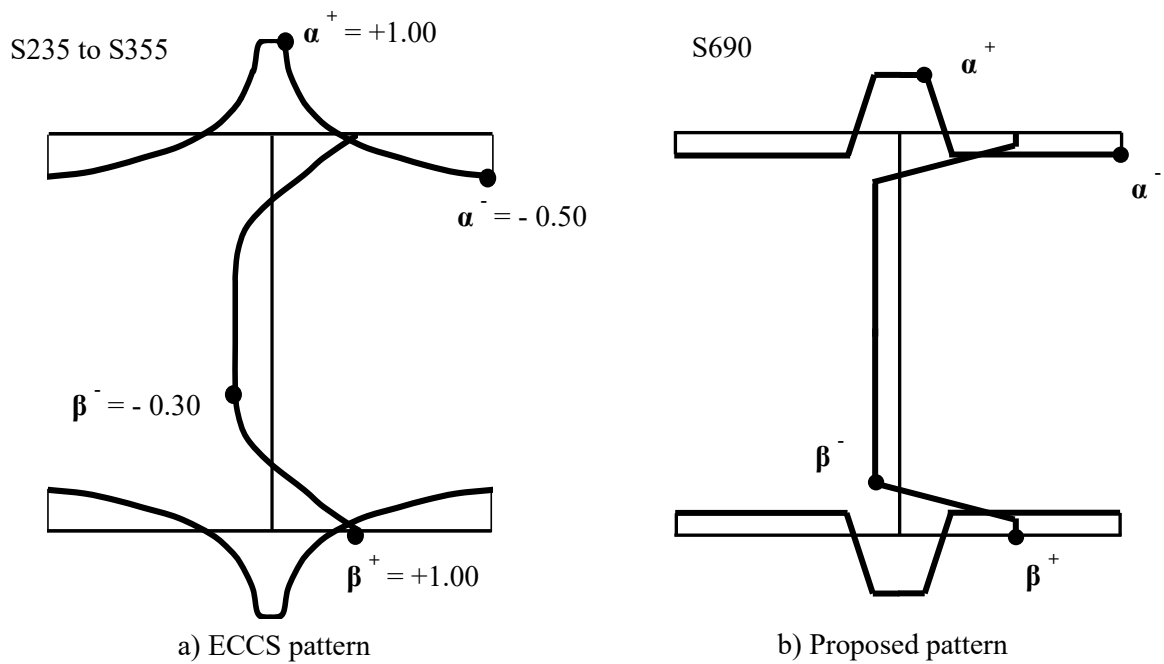
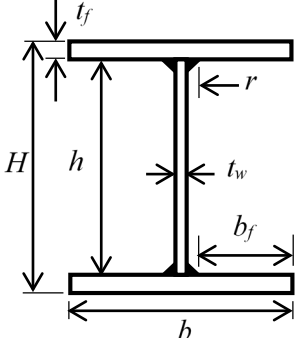


Figure 21. Comparison of simplified residual stress patterns

Table 1 Test programme


Section	Cross-section type	Web thickness, t_w (mm)	Flange thickness, t_f (mm)	Web height, h (mm)	Flange width, b (mm)	Weld size, r (mm)	Length, L (mm)	Welding method
C1	C1	5.83	9.93	119.5	119.6	7.9	899.0	GMAW
C2	C2	5.83	9.94	149.5	149.5	7.5	1000.5	GMAW
C3	C3	9.93	15.98	200.2	199.7	9.8	1250.0	SAW
C4	C4	9.93	15.91	2151.5	250.6	10.5	1450.5	SAW

- Notes: i) Measured dimensions are given.
ii) GMAW denotes gas metal arc manual welding with single pass, and
SAW denotes submerged arc automatic welding with single pass.

Table 2 Mechanical properties of S690 steel plates and electrodes

Item	Young's modulus (kN/mm ²)	Yield strength, f_y (N/mm ²)	Tensile strength, f_u (N/mm ²)	f_u / f_y	Elongation at fracture ϵ_f (%)	Elongation at f_u ≥ 15 (f_y/E)
6 mm thick plate	210.8	780	817	1.05	15.8	Yes
10mm thick plate	215.3	754	800	1.06	16.3	Yes
16mm thick plate	209.5	799	856	1.07	17.3	Yes
CHW-80C1 (for GMAW)	---	700	820	1.17	18.0	---
CHW-S80 (for SAW)	---	710	810	1.14	20.0	---

Table 3 Welding parameters

Section	Pre-heating temperature (°C)	Welding method	Welding parameters			Welding efficiency, η	Heat input energy, Q (kJ/mm)
			Current, I (A)	Voltage, U (V)	Speed, s (mm/s)		
C1	120~150	GMAW	236	29.0	5.0	0.85	1.19
C2	120~150	GMAW	270	30.5	6.3	0.85	1.11
C3	120~150	SAW	450	34.0	5.4	0.95	2.69
C4	120~150	SAW	450	36.0	5.6	0.95	2.75

Table 4 Measured surface residual stresses of a S690 welded H-section - Section C3 (N/mm²)

Points	Outer surface of the top flange (TF)	Outer surface of the bottom flange (BF)	Left surface of the web plate (LW)	Right surface of the web plate (RW)
1	-149	-75	-	-
2	-180	-166	-	-
3	-135	-160	-	-
4	-150	-161	-156	-177
5	-136	-128	-166	-173
6	-101	-106	-94	-147
7	+156	+76	-90	-174
8	+368	+204	-103	-166
9	+54	+11	-103	-151
10	-119	-126	-107	-163
11	-134	-150	-114	-163
12	-154	-134	-121	-116
13	-145	-150	-	-
14	-176	-129	-	-
15	-119	-127	-	-

Note: “+” denotes tensile stress while “-” denotes compressive stress.

Table 5 Measured maximum surface residual stresses

Specimen	Welding method	Flange (tension)				Flange (compression)				Web (compression)			
		$f_{rs,t}$ (test)	f_y (test)	$f_{rs,t} / f_y$ (test)	$f_{rs,t} / f_y$ (ECCS)	$f_{rs,c}$ (test)	f_y (test)	$f_{rs,c} / f_y$ (test)	$f_{rs,c} / f_y$ (ECCS)	$f_{rs,c}$ (test)	f_y (test)	$f_{rs,c} / f_y$ (test)	$f_{rs,c} / f_y$ (ECCS)
Section C1	GMAW	+357	+754	0.47	1.00	-267	+754	-0.35	-0.50	-111	+780	-0.14	-0.30
Section C2	GMAW	+452	+754	0.60	1.00	-250	+754	-0.33	-0.50	-86	+780	-0.11	-0.30
Section C3	SAW	+368	+799	0.46	1.00	-180	+799	-0.23	-0.50	-177	+754	-0.23	-0.30
Section C4	SAW	+354	+799	0.44	1.00	-146	+799	-0.18	-0.50	-152	+754	-0.20	-0.30

Notes:

$f_{rs,t} / f_y$ (test) is related to measured surface residual stresses, and

$f_{rs,t} / f_y$ (ECCS) is an established value adopted assuming residual stresses being uniform across plate thickness.

Table 6 Dimensions and parameters of the double ellipsoidal heat source

Section	Welding method	η	f_f	f_r	a_1 (mm)	a_2 (mm)	b (mm)	c (mm)
C1	GMAW	0.85	0.6	1.4	5.0	7.5	3.0	8.0
C2	GMAW	0.85	0.6	1.4	5.0	7.5	3.0	8.0
C3	SAW	0.95	0.6	1.4	7.5	10.0	5.0	10.0
C4	SAW	0.95	0.6	1.4	7.5	10.0	5.0	10.0

Table 7 Programme of convergence study with various mesh configurations

Section	Nos. of elements				Total nos. of elements
	across flange	across web	across thickness	across length	
C1-a	15	16	1	21	1,218
C1-b	18	18	2	25	3,000
C1-c	25	22	3	30	7,440
C1-d	32	28	4	38	15,808
C1-e	43	38	5	50	35,200
C1-f	64	58	6	75	92,700

Table 8 Results of convergence study with various mesh configurations

Section	Values at the position of Thermocouple T2		Total tensile force at flange/web junction (kN)	Computing time (hour)
	surface temperature (°C)	surface tensile residual stresses (N/mm ²)		
C1-a	---	---	---	---
C1-b	505	+392	+209	9.8
C1-c	506	+407	+217	36.2
C1-d	511	+433	+231	85.1
C1-e	510	+436	+232	261.4
C1-f	511	+434	+231	595.3

Table 9 Validation of measured and predicted surface residual stresses – Section C3 (N/mm²)

Point	Outer surface of the top flange (TF)			Outer surface of the bottom flange (BF)			Left surface of the web (LW)			Right surface of the web (RW)		
	$f_{rs,test}$	$f_{rs,FEM}$	$f_{rs,test}-f_{rs,FEM}$	$f_{rs,test}$	$f_{rs,FEM}$	$f_{rs,test}-f_{rs,FEM}$	$f_{rs,test}$	$f_{rs,FEM}$	$f_{rs,test}-f_{rs,FEM}$	$f_{rs,test}$	$f_{rs,FEM}$	$f_{rs,test}-f_{rs,FEM}$
1	-149	-152	+3	-75	-155	+80	-	-	-	-	-	-
2	-180	-151	-29	-166	-150	-16	-	-	-	-	-	-
3	-135	-151	+16	-160	-146	-14	-	-	-	-	-	-
4	-150	-151	+1	-161	-143	-18	-156	-115	-41	-177	-125	-52
5	-136	-152	+16	-128	-141	+13	-166	-111	-55	-173	-124	-49
6	-101	-150	+49	-106	-134	+28	-94	-109	+15	-147	-121	-26
7	+156	+8	+148	+76	+61	+15	-90	-107	+17	-174	-119	-55
8	+368	+293	+75	+204	+255	-51	-103	-104	+1	-166	-117	-49
9	+54	+148	-94	+11	-18	+29	-103	-102	-1	-151	-117	-34
10	-119	-145	+26	-126	-123	-3	-107	-100	-7	-163	-117	-46
11	-134	-147	+13	-150	-125	-25	-114	-99	-15	-163	-117	-46
12	-154	-146	-8	-134	-124	-10	-121	-100	-21	-116	-117	+1
13	-145	-145	0	-150	-123	-27	-	-	-	-	-	-
14	-176	-145	-31	-129	-123	-6	-	-	-	-	-	-
15	-119	-145	26	-127	-123	-4	-	-	-	-	-	-
Error	$(\sum f_{rs,test}-f_{rs,FEM})/n$		36			23			19			40
	$(\sum (f_{rs,test}-f_{rs,FEM})/f_y)/n$		4.5 %			2.8 %			2.5 %			5.3 %

Note: i) “+” denotes tensile stress while “-” denotes compressive stress.

ii) “n” denotes the total number of measured or predicted data in each part.

Table 10 Average relative errors in predicted surface residual stresses (%)

Section	Outer surface of the top flange (TF)	Outer surface of the bottom flange (BF)	Left surface of the web (LW)	Right surface of the web (RW)	Overall error
C1	7.9	3.9	9.4	11.2	8.1
C2	8.2	6.4	4.5	4.9	6.0
C3	4.5	2.8	2.5	5.3	3.8
C4	2.8	6.1	4.6	3.4	3.9

Table 11 Critical ratios in residual stress patterns

Section	Welding method	Flange thickness, t_f (mm)	Web thickness, t_w (mm)	Residual stress ratios f_{rs}/f_y for S235 to S355 welded sections (recommended by ECCS)				Residual stress ratios f_{rs}/f_y for S690 welded sections (proposed)			
				α^+	α^-	β^+	β^-	α^+	α^-	β^+	β^-
				C1	GMAW	10	6	+1.0	-0.5	+1.0	-0.3
C2	GMAW	10	6	+1.0	-0.5	+1.0	-0.3	+0.82	-0.21	+1.0	-0.20
C3	SAW	16	10	+1.0	-0.5	+1.0	-0.3	+0.58	-0.15	+1.0	-0.16
C4	SAW	16	10	+1.0	-0.5	+1.0	-0.3	+0.57	-0.13	+1.0	-0.13